Signal Processing 210 (2023) 109093

Contents lists available at ScienceDirect

Signal Processing

journal homepage: www.elsevier.com/locate/sigpro

Short communication

Convolution-based free-form deformation for multimodal groupwise registration

Rosa-María Menchón-Lara*, Federico Simmross-Wattenberg, Manuel Rodríguez-Cayetano, Pablo Casaseca-de-la-Higuera, Miguel Á. Martín-Fernández, Carlos Alberola-López

Laboratorio de Procesado de Imagen, ETSI de Telecomunicación, Universidad de Valladolid, Valladolid, Spain

ARTICLE INFO

Article history:
Received 20 October 2022
Revised 10 April 2023
Accepted 3 May 2023
Available online 4 May 2023

Keywords:
Free-form deformation
Multimodal images
Registration
Convolution

ABSTRACT

Recently, an efficient implementation of convolution-based free form deformations (FFD) has been proposed for both groupwise 3D monomodal and 2D pairwise multimodal registrations. However, there is still an unmet need in the field for groupwise L-D multimodal registration with $L \geq 2$. In this correspondence, we address this need and present a solution for achieving accurate registration using two popular metrics: Renyi entropy and PCA2.

1. Introduction

Image registration is the process of aligning multiple images of the same object to a common coordinate system. This process involves applying an image transformation, which can be either rigid or non-rigid [1]. The registration process can be performed pairwise (PW) or groupwise (GW), where PW refers to aligning two images independently, while GW involves aligning a whole set of images jointly. Additionally, the images to be aligned may have the same intensity properties or differ; each case requires different metrics to measure image similarity, thus leading to either monomodal or multimodal registration procedures [1,2].

Free form deformations (FFDs) are widely used to model non-rigid transformations, particularly in medical imaging [3,4]. We recently proposed an efficient convolution-based implementation of FFDs [5] for groupwise non-rigid registration of 3D monomodal images using the sum of squared differences as the image similarity measure. Additionally, in Menchón-Lara et al. [6], we addressed the problem of pairwise multimodal registration in 2D. In this work, we identified a sufficient condition for the gradient metric to be expressed in terms of convolutions and showed that our approach can be applied to commonly used elastic regularization terms and their gradients

In this correspondence, we address the unmet problem of groupwise multimodal non-rigid registration in L-dimensional images. Specifically, we focus on two popular multimodal metrics: the PCA2 metric proposed in Huizinga et al. [7], and the Renyi Entropy metric used in Cordero-Grande et al. [8]. We will demonstrate that these metrics meet the sufficient condition identified in Menchón-Lara et al. [6] that makes them suitable for a convolutional formulation.

The remainder of this paper is organized as follows: Section 2 provides background information on image registration, with a focus on convolution-based formulations for efficient implementation. In Section 3, we demonstrate that the proposed convolution-based formulation applies to the two multimodal metrics mentioned earlier. Section 4 presents the registration results. Finally, Section 5 concludes the paper by summarizing the main contributions. Mathematical details are provided in Appendix A.

2. Background

This section briefly introduces the fundamentals of image registration, focusing on the techniques used in the paper. Specifically, in Section 2.1 the FFD model is discussed, both in its original form and its equivalent convolutional implementation. Then, in Section 2.2 we discuss GW multimodal registration, posed as an optimization problem. A cost function is defined to naturally obtain its gradient, which leads to the sufficient condition mentioned earlier.

2.1. Convolution-based FFD

FFD defines the spatial transformation for a spatial point in the image ($\mathbf{x} \in \mathcal{X} \subset \mathbb{R}^L$) from a grid of control points $\mathbf{u}$ as Rueckert and

* Corresponding author.
E-mail address: rmenchon@lpi.tel.uva.es (R.-M. Menchón-Lara).

https://doi.org/10.1016/j.sigpro.2023.109093

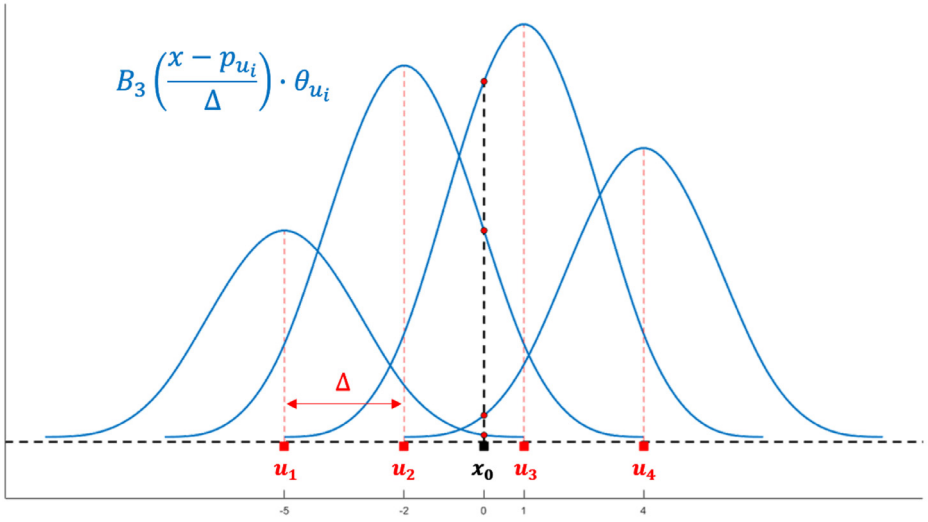

(a) $T(x_0) = x_0 + B\left(\frac{5}{3}\right)\theta_{u_1} + B\left(\frac{2}{3}\right)\theta_{u_2} + B\left(\frac{-1}{3}\right)\theta_{u_3} + B\left(\frac{-4}{3}\right)\theta_{u_4}$

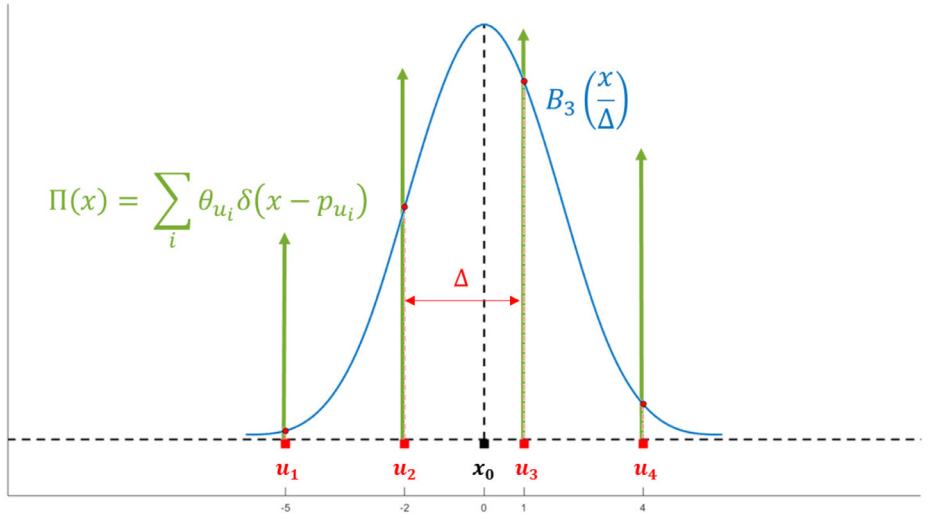

(b) $T(x_0) = x_0 + B\left(\frac{-5}{3}\right)\theta_{u_1} + B\left(\frac{-2}{3}\right)\theta_{u_2} + B\left(\frac{1}{3}\right)\theta_{u_3} + B\left(\frac{4}{3}\right)\theta_{u_4} = x_0 + B\left[\frac{x}{\Delta}\right] * \Pi[x]\big|_{x_0}$

Fig. 1. Graphical interpretation of convolutional implementation of FFD transformations in 1D domain.

Aljabar [4], Lee et al. [9]

$$\mathbf{x}' = \mathbf{T}_{\boldsymbol{\theta}}(\mathbf{x}) = \mathbf{x} + \sum_{\mathbf{u}\in\mathcal{N}(\mathbf{x})} \left(\prod_{l=1}^{L} B\left(\frac{x_l - p_{u_l}}{\Delta_l}\right) \right) \boldsymbol{\theta}_{\mathbf{u}}, \tag{1}$$

where B stands for the B-spline function,[1] $\mathcal{N}(\mathbf{x})$ denotes the set of control points in the vicinity of $\mathbf{x}$, $\boldsymbol{\theta}_{\mathbf{u}} = \{\theta_{u_1}, \ldots, \theta_{u_L}\}$ represents a deformation associated to control point $\mathbf{u}$, p_{u_l} is the location of a given control point in $\mathcal{X}$ along dimension l, and Δ_l is the control point spacing along dimension l. Finally, $\boldsymbol{\theta}$ is the set of $\boldsymbol{\theta}_{\mathbf{u}}$, $\mathbf{u} \in \mathcal{N}(\mathbf{x})$.

Based on the even symmetry and compact support of B-splines, and by defining the grid of control points on a discrete Cartesian coordinate system, the original tensor product formulation in Eq. (1) can be implemented with convolutions [5]. This idea is depicted in Fig. 1, where the equivalence of tensor product and convolutions for a 1D transformation at a generic point x_0 is shown, considering a control point spacing $\Delta = 3$. The influence of each control point is limited to a radius $R = (E+1)\Delta/2$, where $E = 3$ represents the B-spline function order, due to its compact support property. Therefore, as shown in Fig. 1(a), only the four nearest control points are involved in the calculation of $T(x_0)$. Alternatively, the function $\Pi(x)$ can be defined as a series of impulses positioned at the locations of control points and adjusted by the respective deformations θ_u. The transformed point $T(x_0)$ can then be computed by convolving $\Pi(x)$ with the B-spline function $B(x/\Delta)$ evaluated at the point x_0, as shown in Fig. 1(b). It is worth noting that both implementations, the original tensor product formulation in Eq. (1) and the convolution-based implementation using $\Pi(x)$ and $B(x/\Delta)$, are completely equivalent.

The extension to 2D is straightforward, as shown in Menchón-Lara et al. [6]. The 2D transformation can be expressed as two consecutive 1D discrete convolutions with zero extension, where each convolution is performed along a spatial dimension (refer to

[1] We assume third order B-spline functions, due to their good balance between function smoothness and support region.

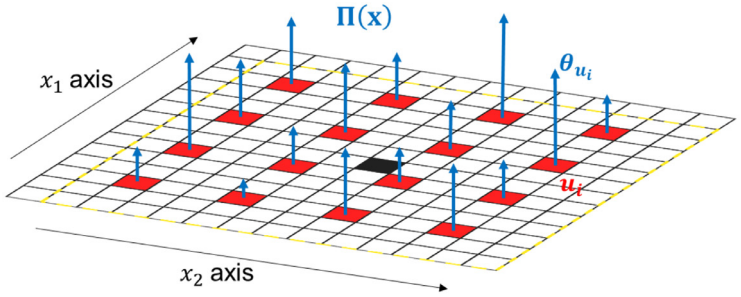

(a) Definition of $\Pi(x)$ function.

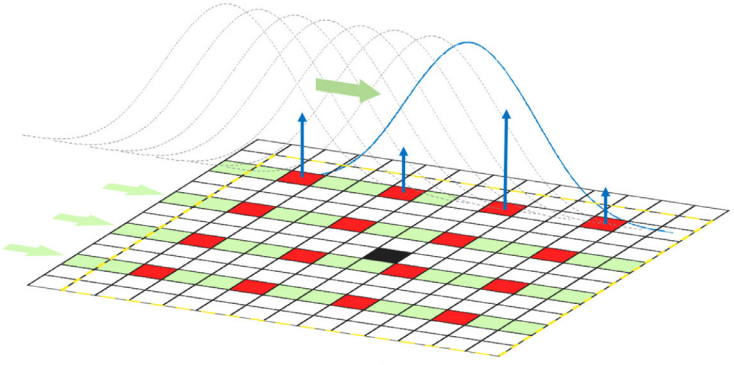

$$\Psi[p_{u_1}, x_2] = B_3\left[\frac{x_2}{\Delta_2}\right] * \Pi[p_{u_1}, x_2]$$

(b) 1D convolution along x_2-axis (only at p_{u_1} locations).

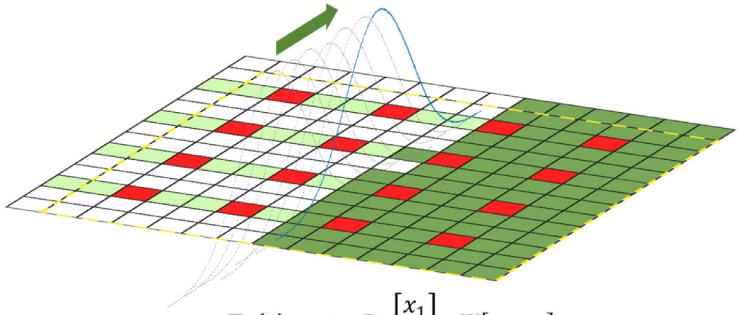

$$\mathbf{T}_{\boldsymbol{\theta}}(\mathbf{x}) = \mathbf{x} + B_3\left[\frac{x_1}{\Delta_1}\right] * \Psi[x_1, x_2]$$

(c) 1D convolution along x_1-axis (whole grid).

Fig. 2. Convolutional formulation for FFD transformations in 2D scenarios.

Fig. 2). Notably, the first convolution is only evaluated in the rows or columns that contain control points.

Likewise, the L-D extension is straightforward due to the separability property of convolutions. Figure 3 illustrates the 3D case, where the 3D tensor product can be reduced to a series of 1D convolutions along each coordinate axis. The following steps show how this is done: (i) a 1D convolution is performed along the x_3-axis, evaluated only at positions (p_{u_1}, p_{u_2}) (Fig. 3(a)); (ii) a second 1D convolution is performed along the x_2-axis, only evaluated at points p_{u_1} (Fig. 3(b)); and finally, (iii) a third 1D convolution is performed along the x_1-axis, evaluated across the entire Cartesian grid (Fig. 3(c)).

2.2. Groupwise multimodal registration

Consider a set of N images $\mathbf{I} = \{I_1, \ldots, I_N\}$, where each image $I_n(\mathbf{x}_n)$ is defined on a finite image domain $\mathbf{x}_n = (x_n^1, \ldots, x_n^L) \in \mathcal{X}_n \subset \mathbb{R}^L$, with $1 \leq n \leq N$. In the context of GW registration, the objective is to determine an optimal set of spatial transformations $\mathcal{T}_{\boldsymbol{\Theta}} = \{\mathbf{T}_{\boldsymbol{\theta}_n} : \mathbf{x}'_n = \mathbf{T}_{\boldsymbol{\theta}_n}(\mathbf{x}) \in \mathcal{X}_n, 1 \leq n \leq N\}$ that map the coordinates of each material point in a common reference space (i.e., $\mathbf{x} \in \mathcal{X}$) to its corresponding coordinates in $\mathcal{X}_n$, with $1 \leq n \leq N$. The registered sequence is then defined as $\mathbf{I}_{\boldsymbol{\Theta}} = \{I_{\boldsymbol{\theta}_1}, \ldots, I_{\boldsymbol{\theta}_N}\}$, with $I_{\boldsymbol{\theta}_n}(\mathbf{x}'_n) = I_n(\mathbf{T}_{\boldsymbol{\theta}_n}(\mathbf{x}))$, $1 \leq n \leq N$. Figure 4 illustrates this process for the case of $L = 2$.

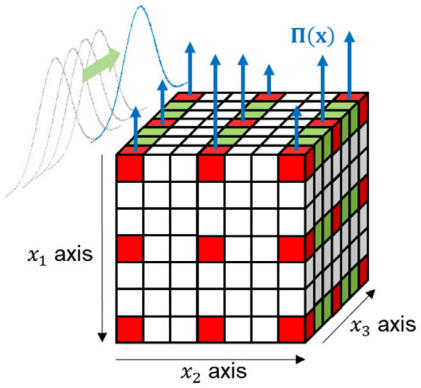

(a) 1D convolution along x_3-axis (only at (p_{u_1}, p_{u_2}) locations).

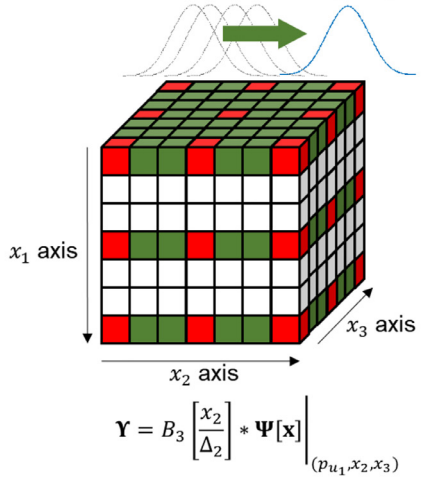

(b) 1D convolution along x_2-axis (only at p_{u_1} locations).

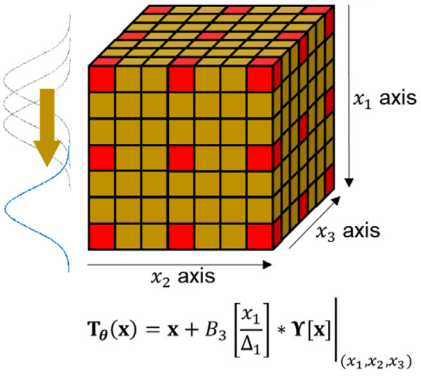

(c) 1D convolution along x_1-axis (whole grid).

Fig. 3. Convolutional implementation for 3D FFD transformations.

The set of deformation parameters, $\boldsymbol{\Theta} = \{\boldsymbol{\theta}_1, \ldots, \boldsymbol{\theta}_N\}$, is optimised by minimizing a cost function that is typically composed of a term $\mathcal{D}(\boldsymbol{\Theta})$ related to the grade of misalignment between the images —the registration metric— and a regularization term $\mathcal{R}(\boldsymbol{\Theta})$ that promotes displacement fields that are physically realistic. Consequently, the problem can be formulated as:

$$\hat{\boldsymbol{\Theta}} = \text{argmin}_{\boldsymbol{\Theta}}\{\mathcal{D}(\boldsymbol{\Theta}) + \mathcal{R}(\boldsymbol{\Theta})\}. \tag{2}$$

The definition of $\mathcal{R}$ leads to the classification of registration methods, including elastic, fluid, diffusion, or curvature registration [2]. In the case of a multimodal problem, the registration metric $\mathcal{D}$ must be able to handle inhomogeneous intensity levels. This is necessary since different acquisition devices or image dynamics may result in varying intensity ranges, such as shadowing in natural landscapes or contrast changes in medical images.

In optimization-based registration methods, the problem described in Eq. (2) is iteratively solved, and the metric gradient with respect to the deformation parameter set ($\nabla\mathcal{D}(\boldsymbol{\Theta})$) needs to be evaluated at each iteration. This computation is typically the most time-consuming part of the registration process. We showed in Menchón-Lara et al. [6] that the gradient can be efficiently computed using convolutions if the partial derivative of the registration metric with respect to each component, θ_{n,u_l}, of the transformation parameters contains terms with the following structure:

$$\sum_{\mathbf{x}\in\mathcal{X}} \Lambda_{\mathcal{D}}(\mathbf{x}) \frac{\partial I_{\boldsymbol{\theta}_n}(\mathbf{x})}{\partial T_{n,l}} \frac{\partial T_{n,l}(\mathbf{x})}{\partial \theta_{n,u_l}}. \tag{3}$$

3. GW multimodal metrics

We analyze in this Section two well-known multimodal metrics suitable for GW multimodal image registration: the Renyi entropy [8] and the PCA2 metric [7]. Our analysis demonstrates that these metrics satisfy the condition outlined in Eq. (3).

3.1. Renyi entropy

Renyi entropy was used as a sparsity-promoting metric by Cordero-Grande et al. [8] for the alignment of contrast-enhanced first-pass perfusion cardiac MRI. This metric is based on the assumption that intensity variations of corresponding points in a time image sequence lead to a sparse representation in a properly selected frame given by a certain decomposition matrix. Specifically, the Renyi entropy of the normalized variable $\hat{z}_k = z_k^2/\|\mathbf{z}\|_2^2$, with $1 \le k \le K$, is defined as

$$\mathcal{D}_{\text{Renyi}}(\mathbf{x}) = \frac{1}{1-\alpha}\log\left(\sum_{k=1}^{K} \hat{z}_k^{\alpha}\right), \tag{4}$$

where $\mathbf{z}$ is a sparse representation of the vector of corresponding intensities, $\mathbf{y} = [y_1 \ldots y_N]^{\mathrm{T}} = \left[I_{\boldsymbol{\theta}_1}(\mathbf{x}) \ldots I_{\boldsymbol{\theta}_N}(\mathbf{x})\right]^{\mathrm{T}}$,

$$\mathbf{z} = \mathbf{W} \cdot \mathbf{y} \tag{5}$$

with $\mathbf{W} \in \mathbb{R}^{K\times N}$, for $K \ge N$, representing a wavelet decomposition matrix. Cordero-Grande et al. [8] recommend the application of an undecimated wavelet transform with a second order Daubechies decomposition and $K = 7N$. The metric $\mathcal{D}(\boldsymbol{\Theta})$ in Eq. (2) is then defined as

$$\mathcal{D}_{\text{Renyi}}(\boldsymbol{\Theta}) = \sum_{\mathbf{x}\in\mathcal{X}} \mathcal{D}_{\text{Renyi}}(\mathbf{x}). \tag{6}$$

Demonstrating that this metric satisfies Eq. (3) is straightforward, as the metric defined on the overall image (as shown in Eq. (6)) is simply the sum of the metric defined at each spatial position $\mathbf{x} \in \mathcal{X}$, i.e.,

$$\begin{aligned}\frac{\partial \mathcal{D}_{\text{Renyi}}(\boldsymbol{\Theta})}{\partial \theta_{n,u_l}} &= \sum_{\mathbf{x}\in\mathcal{X}} \frac{\partial \mathcal{D}_{\text{Renyi}}(\mathbf{x})}{\partial y_n} \cdot \frac{\partial y_n(\mathbf{x})}{\partial T_{n,l}} \cdot \frac{\partial T_{n,l}(\mathbf{x})}{\partial \theta_{n,u_l}} \\ &= \sum_{\mathbf{x}\in\mathcal{X}} \Lambda^{n}_{\text{Renyi}}(\mathbf{x}) \cdot \frac{\partial I_{\boldsymbol{\theta}_n}(\mathbf{x})}{\partial T_{n,l}} \cdot \frac{\partial T_{n,l}(\mathbf{x})}{\partial \theta_{n,u_l}},\end{aligned} \tag{7}$$

with $\Lambda^{n}_{\text{Renyi}}(\mathbf{x})$ defined as

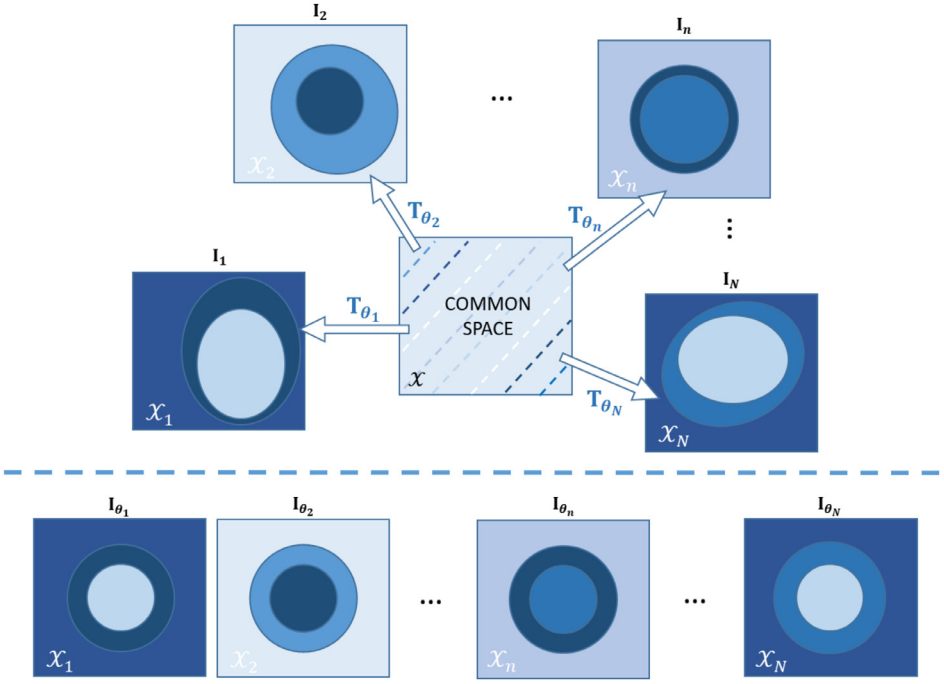

Fig. 4. Scheme of spatial transformations in 2D groupwise multimodal image registration.

$$\Lambda^{n}_{\text{Renyi}}(\mathbf{x}) = \frac{2\alpha}{(1-\alpha)\cdot\|\mathbf{z}\|_2^2\cdot\sum_k \hat{z}_k^{\alpha}} \sum_{k=1}^{K}\left(W_{k,n}\cdot z_k\cdot\hat{z}_k^{\alpha-1} - \hat{z}_k^{\alpha}\sum_{q=1}^{K} W_{q,n}\cdot z_q\right), \tag{8}$$

where he have omitted the dependence on $\mathbf{x}$ through z_k for simplicity.

3.2. PCA2 metric

Huizinga et al. introduced the PCA2 metric for quantitative MRI in Huizinga et al. [7]. The metric operates on the premise that intensities of corresponding points undergo changes following a low-dimensional model. Hence, when an image becomes misaligned, there is a mismatch in the model, which the metric aims to quantify. Specifically, for an N-image set, the degree of this mismatch is quantified by

$$\mathcal{D}_{\text{PCA2}}(\boldsymbol{\Theta}) = \sum_{j=1}^{N} j\cdot\lambda_j, \tag{9}$$

where λ_j, refers to the jth eigenvalue of the correlation matrix $\mathbf{C}\in\mathbb{R}^{N\times N}$ of the transformed images (note that $\lambda_j > \lambda_{j+1}$). The correlation matrix can be defined as Huizinga et al. [7]

$$\mathbf{C} = \frac{1}{|\mathcal{X}|-1}\boldsymbol{\Sigma}^{-1}(\mathbf{M}-\overline{\mathbf{M}})^{\mathrm{T}}(\mathbf{M}-\overline{\mathbf{M}})\boldsymbol{\Sigma}^{-1}, \tag{10}$$

where $|\mathcal{X}|$ is the number of per-image elements, $\mathbf{M}\in\mathbb{R}^{|\mathcal{X}|\times N}$ is a matrix that contains the transformed images $\{I_{\boldsymbol{\theta}_n}, n=1,\ldots,N\}$ as column vectors, $\boldsymbol{\Sigma}$ is a diagonal matrix with the standard deviations of each column of $\mathbf{M}$, and $\overline{\mathbf{M}} = (\frac{1}{N}\mathbf{M}\mathbf{1}_N)\mathbf{1}_N^T$, where $\mathbf{1}_N$ is an N-column vector of ones.

The derivative of PCA2 with respect to the deformation parameters can be expressed as Huizinga et al. [7], van der Aa et al. [10]

$$\frac{\partial\mathcal{D}_{\text{PCA2}}(\boldsymbol{\Theta})}{\partial\theta_{n,u_l}} = \sum_{j=1}^{N} j\boldsymbol{v}_j^{\mathrm{T}}\frac{\partial\mathbf{C}}{\partial\theta_{n,u_l}}\boldsymbol{v}_j, \tag{11}$$

where $\boldsymbol{v}_j$ stands for the jth eigenvector of $\mathbf{C}$. Albeit a matrix description of this expression based on the formulation in Eq. (10) is detailed in Huizinga et al. [7], our focus will be on Eq. (11) to check whether the sufficient condition is satisfied. Specifically,

$$\mathbf{C} = \begin{bmatrix} \rho_{1,1} & \rho_{1,2} & \cdots & \rho_{1,N} \\ \vdots & \vdots & \ddots & \vdots \\ \rho_{N,1} & \rho_{N,2} & \cdots & \rho_{N,N} \end{bmatrix} \tag{12}$$

with

$$\rho_{i,j} = \frac{1}{|\mathcal{X}|-1}\sum_{\mathbf{x}\in\mathcal{X}}\left(\frac{I_{\boldsymbol{\theta}_i}(\mathbf{x})-\mu_i}{\sigma_i}\right)\left(\frac{I_{\boldsymbol{\theta}_j}(\mathbf{x})-\mu_j}{\sigma_j}\right), 1\le i,j\le N, \tag{13}$$

where μ_n, σ_n stand for the average and standard deviation of $I_{\boldsymbol{\theta}_n}$, respectively.

Calculating the PCA2 gradient requires the derivative of the correlation matrix, which, in turn, needs the computation of the derivatives of the correlation coefficients. For a detailed formulation of these derivatives, please refer to Appendix A. The outcome of these calculations is:

$$\frac{\partial\rho_{i,n}}{\partial\theta_{n,u_l}} = \sum_{\mathbf{x}\in\mathcal{X}}\Lambda^{i,n}_{\text{PCA2}}(\mathbf{x})\frac{\partial I_{\boldsymbol{\theta}_n}(\mathbf{x})}{\partial T_{\theta_{n,l}}}\frac{\partial T_{\theta_{n,l}}(\mathbf{x})}{\partial\theta_{n,u_l}} \tag{14}$$

with

$$\Lambda^{i,n}_{\text{PCA2}}(\mathbf{x}) = \frac{1}{(|\mathcal{X}|-1)\sigma_n}\left[\left(\frac{I_{\boldsymbol{\theta}_i}(\mathbf{x})-\mu_i}{\sigma_i}\right) - \rho_{i,n}\left(\frac{I_{\boldsymbol{\theta}_n}(\mathbf{x})-\mu_n}{\sigma_n}\right)\right]. \tag{15}$$

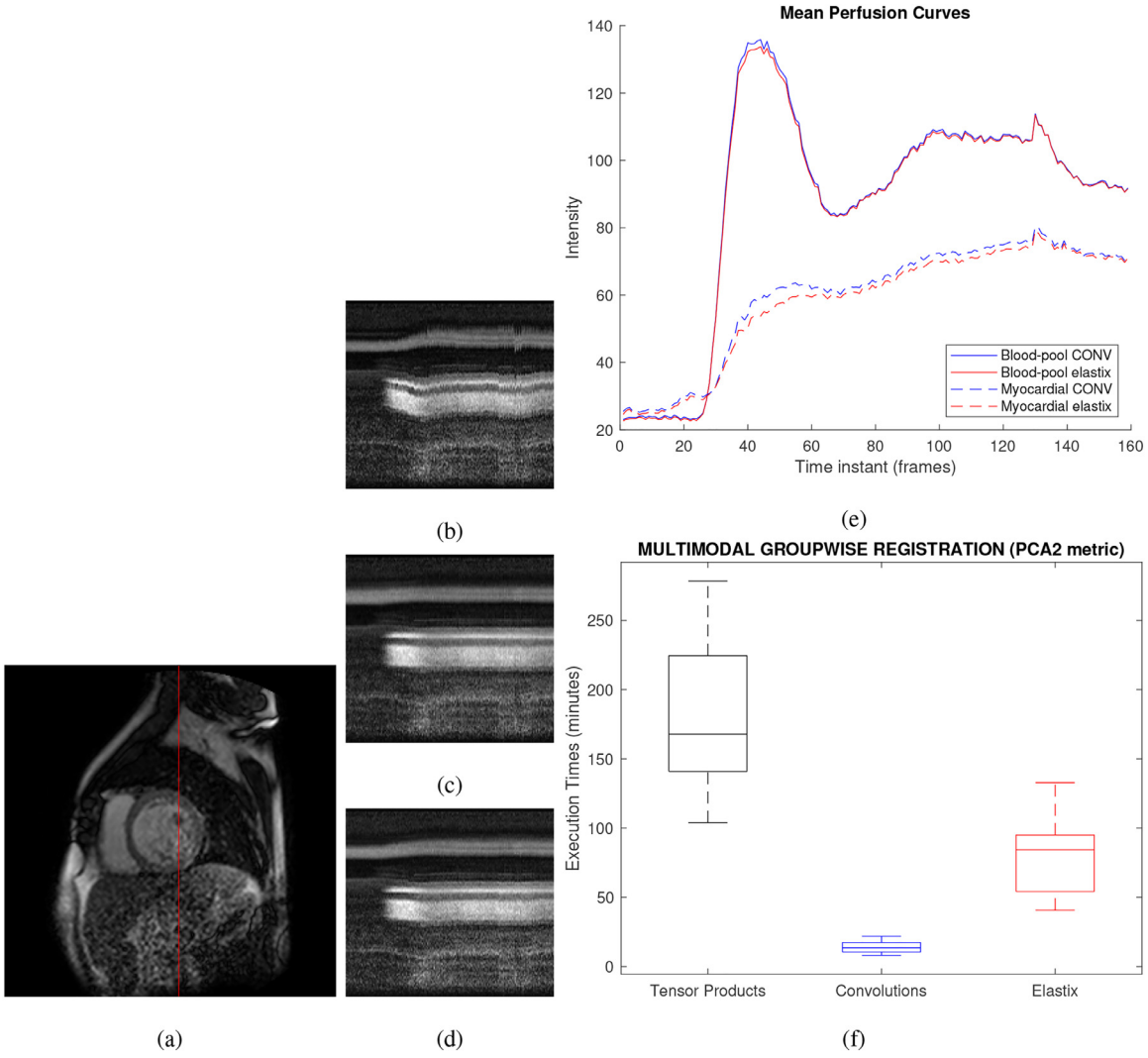

Fig. 5. Results for groupwise registration of dynamic cardiac perfusion MRI using PCA2 metric: (a) Example image frame with selected vertical profile (red line); (b) temporal profile on the original sequence; (c) temporal profile of the registered sequence using the proposed method; (d) temporal profile of the registered sequence using elastix; (e) mean perfusion curves at blood-pool (solid) and myocardium (dashed) after registration with the proposed convolutional method (blue) and Elastix (red); (f) boxplot of GW registration times on CPU in minutes for the dataset described in Menchón-Lara et al. [6] using the proposed convolutional implementation, the classical tensor product formulation, and Elastix.

Hence, Eq. (11) becomes

$$\frac{\partial \mathcal{D}_{\mathrm{PCA2}}(\boldsymbol{\Theta})}{\partial \theta_{n,u_l}} = \sum_{\mathbf{x}\in\mathcal{X}} \underbrace{\left[\sum_{j=1}^{N} j \cdot \boldsymbol{v}_j^{\mathrm{T}} \boldsymbol{\Lambda}_{\mathrm{PCA2}}(\mathbf{x}) \boldsymbol{v}_j\right]}_{\Lambda_{\mathcal{D}}(\mathbf{x})} \frac{\partial I_{\boldsymbol{\theta}_n}(\mathbf{x})}{\partial T_{\theta_{n,l}}} \frac{\partial T_{\theta_{n,l}}(\mathbf{x})}{\partial \theta_{n,u_l}} \tag{16}$$

with $\boldsymbol{\Lambda}_{\mathrm{PCA2}}(\mathbf{x})$ a $N \times N$ matrix whose (i,n) element is $\Lambda^{i,n}_{\mathrm{PCA2}}(\mathbf{x})$.

4. Results

To illustrate the method's performance, we evaluated the PCA2 metric using the cardiac perfusion MRI dataset described in Menchón-Lara et al. [6]. We employed the nonlinear conjugate gradient descent algorithm using *MATLAB R2020a*. For the sake of comparison, we used Elastix[2] as reference. It was adapted to GW operation mode using a single resolution level, random coordinate undersampling strategy, and adaptive stochastic gradient descent optimization. Figure 5 shows an example of an aligned sequence. Figure 5(b)–(d) show the temporal intensity profiles corresponding to the red line marked in Fig. 5(a) for both the original non registered sequence, and the aligned sequences using our convolutional method and Elastix, respectively. The mean perfusion curves in the blood-pool and in the myocardium obtained after registration using both tools are shown in Fig. 5(e). Finally, Fig. 5(f) shows boxplots of the execution times with tensor products, Elastix and our method. Figure 6 shows average perfusion curves from pixels at the standard zones defined in the myocardium. In this case, together with the unregistered sequence (solid black), Elastix (solid red) and our method (solid blue), the results of PW registration with different images used as a reference are also shown in yellow dotted lines, which reveal the dependence on the selected reference. GW approaches (Elastix and ours) eliminate this undesirable effect.

[2] http://elastix.isi.uu.nl/

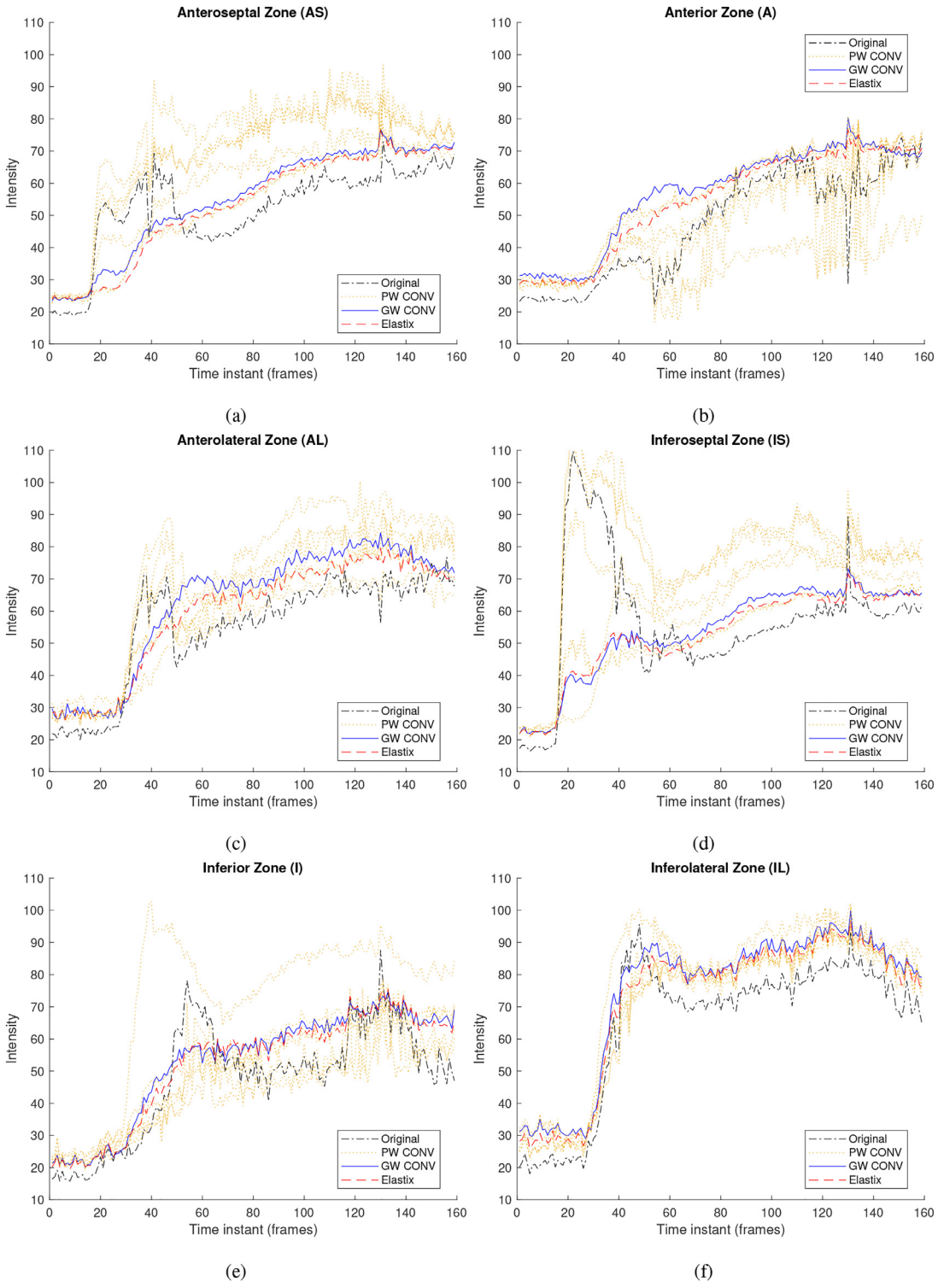

Fig. 6. Myocardial perfusion curves for the image in Fig. 5(a) in the standard zones considered for perfusion analysis. Mean perfusion curves obtained after groupwise image registration using the proposed method with PCA2 metric (blue solid lines) can be compared with the corresponding curves obtained after GW Elastix registration (red dashed lines) and after PW convolutional registration using normalized cross correlation metric and different reference images (yellow dotted lines). The original curves from the non-aligned sequence are also included (black dashed lines).

5. Conclusions

This work addresses the efficient implementation of FFD-based registration. The implementation relies on a reformulation of spatial transformations and gradients via simple 1D convolutions that are successively applied along each dimension of the image domain. This method led to significant run time reductions on both GW monomodal [5] and PW 2D multimodal [6] registration. In this correspondence we addressed the extension of the convolutional strategy for L-D GW multimodal non-rigid registration, which has been missing thus far. To accomplish this, we studied two multimodal GW metrics: Renyi entropy [8], and PCA2 [7]. Our analysis

reveals that both metrics satisfy the sufficient condition identified in Menchón-Lara et al. [6] for the application of the convolutional strategy.

Declaration of Competing Interest

The authors declare that they have no known competing financial interests or personal relationships that could have appeared to influence the work reported in this paper.

CRediT authorship contribution statement

Rosa-María Menchón-Lara: Conceptualization, Investigation, Methodology, Software, Visualization, Writing – original draft. **Federico Simmross-Wattenberg:** Data curation, Resources, Writing – review & editing. **Manuel Rodríguez-Cayetano:** Writing – review & editing. **Pablo Casaseca-de-la-Higuera:** Writing – review & editing. **Miguel Á. Martín-Fernández:** Formal analysis, Writing – review & editing. **Carlos Alberola-López:** Conceptualization, Formal analysis, Project administration, Supervision, Writing – original draft.

Data availability

No data was used for the research described in the article.

Acknowledgments

This work is partially supported by the Spanish '*Ministerio de Economía, Industria y Competitividad*' under grants TEC2017-82408-R and PID2020-115339RB-I00, and by ESAOTE Ltd. under grant 18IQBM.

Appendix A. Convolution-based PCA2 gradient

The derivatives of the correlation coefficients $\rho_{i,j}, 1 \le i, j \le N$ with respect to each element of the deformation parameters (θ_{n,u_l}) are detailed here. Note that $\rho_{i,j} = \rho_{j,i}$, and therefore, $\frac{\partial \rho_{i,n}}{\partial \theta_{n,u_l}} = \frac{\partial \rho_{n,i}}{\partial \theta_{n,u_l}}, 1 \le i \le N$. We can express these derivatives as

$$\left.\frac{\partial \rho_{i,n}}{\partial \theta_{n,u_l}}\right|_{i\neq n} = \frac{1}{|\mathcal{X}|-1}\sum_{\mathbf{x}\in\mathcal{X}}\left[\left(\frac{I_{\boldsymbol{\theta}_i}(\mathbf{x})-\mu_i}{\sigma_i}\right)\cdot\frac{\partial}{\partial\theta_{n,u_l}}\left(\frac{I_{\boldsymbol{\theta}_n}(\mathbf{x})-\mu_n}{\sigma_n}\right)\right] =$$

$$= \frac{1}{|\mathcal{X}|-1}\sum_{\mathbf{x}\in\mathcal{X}}\left(\frac{I_{\boldsymbol{\theta}_i}(\mathbf{x})-\mu_i}{\sigma_i}\right)\cdot\frac{1}{\sigma_n^2}\cdot\left[\left(\frac{\partial I_{\boldsymbol{\theta}_n}(\mathbf{x})}{\partial\theta_{n,u_l}}-\frac{\partial\mu_n}{\partial\theta_{n,u_l}}\right)\sigma_n - \frac{\partial\sigma_n}{\theta_{n,u_l}}\cdot(I_{\boldsymbol{\theta}_n}(\mathbf{x})-\mu_n)\right], \tag{A.1}$$

where

$$\frac{\partial\mu_n}{\partial\theta_{n,u_l}} = \frac{1}{|\mathcal{X}|}\sum_{\mathbf{x}\in\mathcal{X}}\frac{\partial I_{\boldsymbol{\theta}_n}(\mathbf{x})}{\partial\theta_{n,u_l}}, \text{ and}$$

$$\frac{\partial\sigma_n}{\theta_{n,u_l}} = \frac{1}{|\mathcal{X}|-1}\sum_{x\in\mathcal{X}}\left(\frac{I_{\boldsymbol{\theta}_n}(\mathbf{x})-\mu_n}{\sigma_n}\right)\frac{\partial I_{\boldsymbol{\theta}_n}(\mathbf{x})}{\partial\theta_{n,u_l}}.$$

Therefore, the derivatives in Eq. (A.1) can be expressed as

$$\frac{\partial\rho_{i,n}}{\partial\theta_{n,u_l}} = \sum_{\mathbf{x}\in\mathcal{X}}\underbrace{\frac{1}{(|\mathcal{X}|-1)\sigma_n}\left[\left(\frac{I_{\boldsymbol{\theta}_i}(\mathbf{x})-\mu_i}{\sigma_i}\right)-\rho_{i,n}\left(\frac{I_{\boldsymbol{\theta}_n}(\mathbf{x})-\mu_n}{\sigma_n}\right)\right]}_{\Lambda^{i,n}_{\mathrm{PCA2}}}$$

$$\frac{\partial I_{\boldsymbol{\theta}_n}(\mathbf{x})}{\partial T_{\theta_{n,l}}}\frac{\partial T_{\theta_{n,l}}(\mathbf{x})}{\partial\theta_{n,u_l}}. \tag{A.2}$$

For diagonal elements $(i = n)$, the derivatives turn out to be null, since

$$\rho_{n,n} = \frac{1}{|\mathcal{X}|-1}\sum_{\mathbf{x}\in\mathcal{X}}\frac{(I_{\boldsymbol{\theta}_n}(\mathbf{x})-\mu_n)^2}{\sigma_n^2} = \frac{\sigma_n^2}{\sigma_n^2} = 1. \tag{A.3}$$

References

[1] B. Zitová, J. Flusser, Image registration methods: a survey, Image Vis. Comput. 21 (11) (2003) 977–1000, doi:10.1016/S0262-8856(03)00137-9.
[2] B. Fischer, J. Modersitzki, A unified approach to fast image registration and a new curvature based registration technique, Linear Algebra Appl. 380 (2004) 107–124, doi:10.1016/j.laa.2003.10.021.
[3] A. Sotiras, et al., Deformable medical image registration: a survey, IEEE Trans. Med. Imaging 32 (7) (2013) 1153–1190, doi:10.1109/TMI.2013.2265603.
[4] D. Rueckert, P. Aljabar, Non-Rigid Registration Using Free-Form Deformations, Springer US, Boston, MA, 2015, pp. 277–294.
[5] R.-M. Menchón-Lara, et al., Fast 4D elastic group-wise image registration. Convolutional interpolation revisited, Comput. Methods Prog. Biomed. 200 (2021) 105812, doi:10.1016/j.cmpb.2020.105812.
[6] R.-M. Menchón-Lara, et al., Efficient convolution-based pairwise elastic image registration on three multimodal similarity metrics, Signal Process. 202 (2023) 108771, doi:10.1016/j.sigpro.2022.108771.
[7] W. Huizinga, et al., PCA-based groupwise image registration for quantitative MRI, Med. Image Anal. 29 (2016) 65–78, doi:10.1016/j.media.2015.12.004.
[8] L. Cordero-Grande, et al., Groupwise elastic registration by a new sparsity-promoting metric: application to the alignment of cardiac magnetic resonance perfusion images, IEEE Trans. Pattern Anal. 35 (11) (2013) 2638–2650, doi:10.1109/TPAMI.2013.74.
[9] S. Lee, et al., Scattered data interpolation with multilevel b-splines, IEEE Trans. Vis. Comput. Graph. 3 (3) (1997) 228–244, doi:10.1109/2945.620490.
[10] N.P. van der Aa, et al., Computation of eigenvalue and eigenvector derivatives for a general complex-valued eigensystem, Electron. J. Linear Algebra 16 (2007) 300–314, doi:10.13001/1081-3810.1203.